Supplementary information for

Elastic properties of majoritic garnet inclusions in diamonds and the seismic signature of pyroxenites in the Earth's upper mantle

Koemets I., Satta N., Marquardt H., Kiseeva E.S.*, Kumosov A., Stachel T., Harris J., Dubrovinsky L.
*kate.kiseeva@ucc.ie

Methods

Pressure and ferric iron content of majoritic garnets. An estimation of the pressure of last equilibration for the here-studied samples was made following the Beyer and Frost (2017) geobarometer. The uncertainty in calculated pressure that is related to different Y-site Fe content obtained by XRD and $Fe^{3+}/\Sigma Fe$ ratio from Mössbauer spectroscopy from (Beyer and Frost, 2017) is an order of magnitude smaller than the standard deviation of σ=0.86 GPa proposed by Beyer and Frost (2017).

Supplementary Tables

Supplementary Table 1. Composition and Fe^{3+} content of the studied natural majorites (Kiseeva et al., 2018; Tappert et al., 2005). Pressure of last equilibration is calculated using Beyer and Frost geobarometer (Beyer and Frost, 2017). For justification of the proposed geobarometer, please, see Kiseeva et al. (2018).

Major oxides, wt%	JF 37B	JF 39A	JF 55A
SiO_2	42.40	45.20	48.00
TiO_2	0.18	0.31	0.36
Al_2O_3	20.70	15.00	12.10
Cr_2O_3	0.13	0.24	0.36
FeO	11.35	8.64	6.51
Fe_2O_3	1.72	2.40	3.10
MnO	0.38	0.24	0.25
MgO	16.90	20.30	22.00
CaO	6.43	5.67	7.33
Na_2O	0.14	0.37	0.43
P_2O_5	0.02	0.03	0.03
Total	100.36	98.39	100.47
Fe^{3+} by SMS,%	12(3)	20(1)	30(3)
Y-side Fe by XRD.%	7.8(4)	18(4)	25.9(5)
Fe total as FeO	12.9	10.8	9.3
Pressure of last equilibration (GPa)	7.7(9)	13.5(9)	15.6(9)
Cations			
Si	3.068	3.296	3.416
Ti	0.010	0.017	0.019
Al	1.766	1.290	1.015
Cr	0.007	0.014	0.020
Fe^{2+}	0.687	0.527	0.387
Fe^{3+}	0.094	0.132	0.166
Mn	0.023	0.015	0.015
Mg	1.822	2.206	2.333
Ca	0.499	0.443	0.559
Na	0.020	0.052	0.059
P	0.001	0.002	0.002
Total	7.997	7.993	7.991

Supplementary Table 2. Summary of physical parameters of the mineral species used to model mantle rocks. Physical parameters of modelled garnets were calculated from end-member data. Subscripts refer to the assumed end-member molar fractions. Py (Pyrope - Chantel et al. (2016)), Al (Almandine - Arimoto et al. (2015)), Gr (Grossular - Kono et al., 2010), Mj (Mg-Majorite – Liu et al. (2019)) and Uv (Uvarovite - Bass (1986)). Vp* and Vs* are calculated velocities for the here-measured samples based on the end-member fractions reported in Table 1. The measured and calculated sound velocities are in a good agreement. Note that there is a strong velocity contrast between peridotite and pyroxenite, even though P-waves propagate faster (~1.2%) in peridotitic garnet than in our pyroxenitic sample. Compared to pyroxenitic garnet, peridotitic garnet has higher contents of the fastest garnet end-members grossular and pyrope and lower almandine (slowest garnet end-member).

Reference	Mineral	ρ (g cm^{-3})	K_s (GPa)	G (GPa)	V_p (km s^{-1})	V_s (km s^{-1})	$*V_p$ (km s^{-1})	$*V_s$ (km s^{-1})
Our study	JF 37b	3.774(5)	167(1)	94.6(5)	8.81(2)	5.01(1)	8.84(2)	4.96(1)
Our study	JF 39a	3.738(5)	165(1)	91.5(5)	8.77(1)	4.95(1)	8.80(2)	4.93(1)
Our study	JF 55a	3.701(5)	166(3)	92.2(10)	8.84(5)	4.99(3)	8.79(2)	4.93(1)
Abramson et al. (1997)	Olivine	3.355	129.4(6)	78.2(3)	8.35(1)	4.83(1)		
Buchen et al. (2018)	Wadsleyite	3.598(11)	168.0(9)	104.3(5)	9.24(2)	5.38(2)		
Zhang and Bass (2016)	Peridotitic orthopyroxene	3.288(4)	113(1)	75.9(7)	8.07(3)	4.81(2)		
Collins, M. D., & Brown, J. M. (1998)	Peridotitic clinopyroxene	3.327(3)	117.2(7)	72.2(2)	8.01(2)	4.66(1)		
Bhagat et al. (1992)	Na-Omphacite	3.327(2)	130.8(5)	79.2(2)	8.43(1)	4.88(1)		
Hao et al. (2019)	Ca-omphacite	3.339(2)	122(3)	74(2)	8.13(4)	4.70(3)		
Modelled	Py$_{55}$Al$_{20}$Gr$_{16}$M	3.724(4)	170.9(14)	92.8(5)	8.90(2)	4.99(1)		

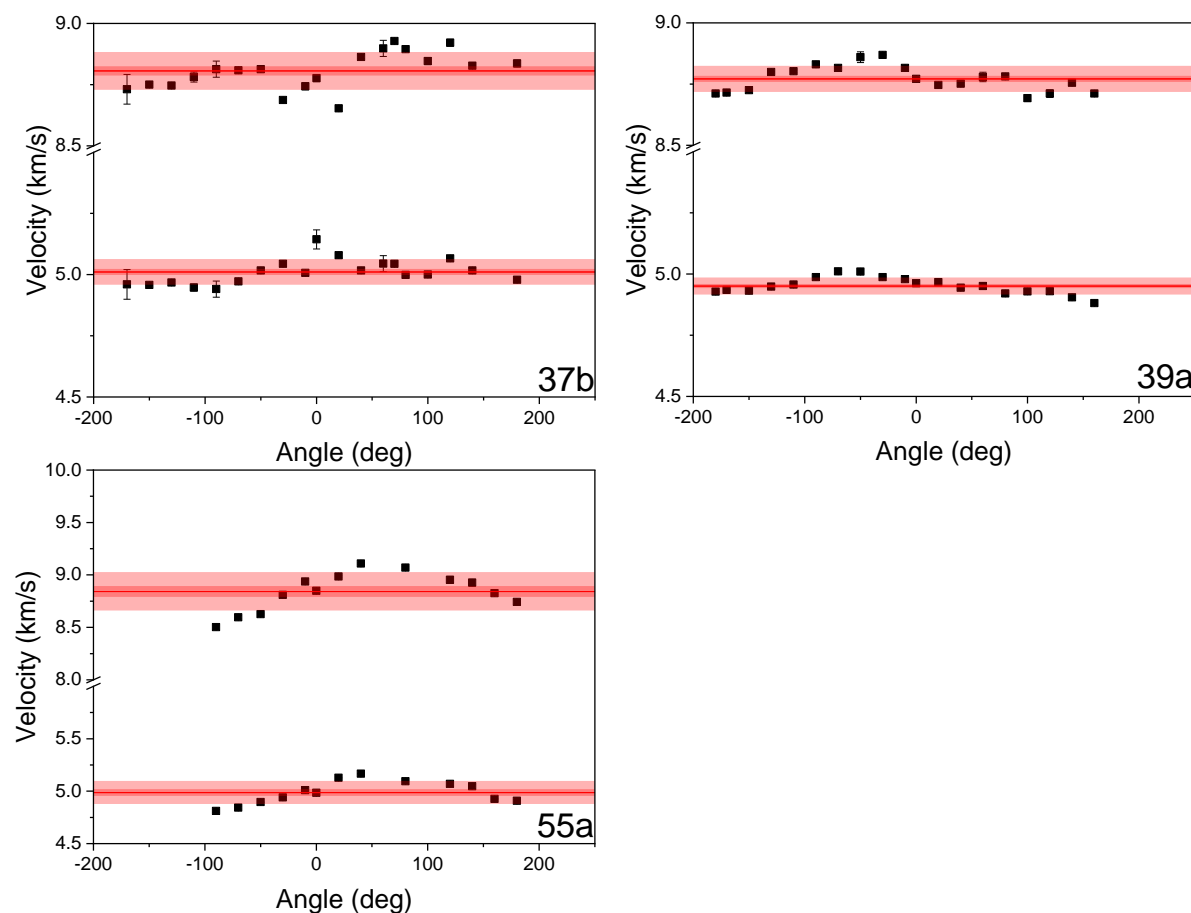|								
garnet	j_7Uv_2							
Modelled garnet	$Py_{33}Al_{30}Gr_{30}Mj_7$	3.798(3)	171.1(12)	96.0(4)	8.87(2)	5.03(1)		
Modelled garnet	$Py_{16}Al_{28}Gr_{26}Mj_{30}$	3.771(3)	167.8(14)	93.7(5)	8.81(2)	4.99(1)		
Modelled garnet	$Py_{44}Al_{13}Gr_{11}Uv_2Mj_{30}$	3.658(4)	167.6(16)	90.1(6)	8.87(3)	4.96(2)		
Modelled garnet	$Py_{35}Al_{11}Gr_{10}Uv_2Mj_{42}$	3.637(4)	165.9(16)	89.1(7)	8.85(3)	4.95(2)		
Modelled garnet	$Py_{14}Al_{22}Gr_{22}UMj_{42}$	3.719(4)	166.1(15)	91.9(6)	8.81(3)	4.97(2)		

Supplementary Table 3. Mineral volume fractions assumed to model mantle rocks. Listed mineral fractions of peridotite and eclogite rocks are based on Frost (2008) and Irifune et al. (1986), respectively. Ol = olivine; P-Cpx = peridotitic clinopyroxene; P-OPx = peridotitic orthopyroxene; Na-Omp = Na-Omphacite; Ca-Omp = Ca-Omphacite; Wd = wadsleyite.

Mantle rocks at 8 GPa	JF 37b	Ol	P-Opx	P-Cpx	E-Na-Cpx	$Py_{55}Al_{20}Gr_{16}Mj_7Uv_2$	$Py_{33}Al_{30}Gr_{30}Mj_7$
Pyroxenite	100						
Peridotite		56	9	15		20	
Eclogite					70		30
Mantle rocks at 13 GPa	JF 39a	Ol	P-Cpx	E-Ca-Cpx	$Py_{16}Al_{28}Gr_{26}Mj_{30}$	$Py_{44}Al_{13}Gr_{11}Uv_2Mj_{30}$	
Pyroxenite	100						
Peridotite		56	10			34	
Eclogite				35	65		
Mantle rocks at 16 GPa	JF 55a	Wd	$Py_{35}Al_{11}Gr_{10}Uv_2Mj_{42}$	$Py_{14}Al_{22}Gr_{22}UMj_{42}$			
Pyroxenite	100						
Peridotite		56	44				
Eclogite				100			

Supplementary Figure

Supplementary Figure 1. Measured individual sound velocities versus chi angle.
Light pink area shows standard deviation of average sound velocity, dark pink shows
standard error.

The original samples had the random shape and in order to prepare the perfect platelet, one
would need to polish away significant portion of unique sample material, which would be too
prodigal just for the Brillouin measurements. Moreover, further polishing create a great rick
of sample destruction.

As a compromise between data quality and sample preservation, we used the least amount of
polishing possible and compensated it with a large amount of measurements. Polished surface
had relatively small area along with significant thickness; this resulted in deviations from
ideal platelet geometry. To minimise the uncertainties, we performed the measurements in all

possible directions (360 degrees rotation with a step of 20 degrees), even though one measurement is enough for isotropic samples in case of ideal platelet geometry. We used standard deviation from all measurements as an upper limit of uncertainty estimation, in case of sample 37b and 39a it did not exceed 1%. In the sample 55a the sound velocities standard deviation of ~2%.

References

Abramson, E.H., Brown, J.M., Slutsky, L.J., Zaug, J.M., 1997. The elastic constants of San Carlos olivine to 17 GPa. Journal of Geophysical Research-Solid Earth 102, 12253-12263.

Arimoto, T., Greaux, S., Irifune, T., Zhou, C.Y., Higo, Y., 2015. Sound velocities of $Fe_3Al_2Si_3O_{12}$ almandine up to 19 GPa and 1700 K. *Physics of the Earth and Planetary Interiors* 246, 1-8.

Bass, J.D., 1986. Elasticity of Uvarovite and Andradite Garnets. *Journal of Geophysical Research-Solid Earth and Planets* 91, 7505-7516.

Beyer, C., Frost, D.J., 2017. The depth of sub-lithospheric diamond formation and the redistribution of carbon in the deep mantle. *Earth and Planetary Science Letters* 461, 30-39.

Bhagat, S.S., Bass, J.D., Smyth, J.R., 1992. Single-Crystal Elastic Properties of Omphacite-C2/C by Brillouin Spectroscopy. *Journal of Geophysical Research-Solid Earth* 97, 6843-6848.

Buchen, J., Marquardt, H., Speziale, S., Kawazoe, T., Ballaran, T.B., Kurnosov, A., 2018. High-pressure single-crystal elasticity of wadsleyite and the seismic signature of water in the shallow transition zone. *Earth and Planetary Science Letters* 498, 77-87.

Chantel, J., Manthilake, G.M., Frost, D.J., Beyer, C., Ballaran, T.B., Jing, Z.C., Wang, Y.B., 2016. Elastic wave velocities in polycrystalline $Mg_3Al_2Si_3O_{12}$-pyrope garnet to 24 GPa and 1300 K. *American Mineralogist* 101, 991-997.

Collins, M.D., Brown, J.M., 1998. Elasticity of an upper mantle clinopyroxene. *Physics and Chemistry of Minerals* 26, 7-13.

Frost, D.J., 2008. The upper mantle and transition zone. *Elements* 4, 171-176.

Hao, M., Pierotti, C. E., Tkachev, S., Prakapenka, V., & Zhang, J. S. 2019. The single-crystal elastic properties of the jadeite-diopside solid solution and their implications for the composition-dependent seismic properties of eclogite. *American Mineralogist*, 104(7), 1016-1021.

Irifune, T., Sekine, T., Ringwood, A.E., Hibberson, W.O., 1986. The eclogite-garnetite transformation at high-pressure and some geophysical implications. *Earth and Planetary Science Letters* 77, 245-256.

Jiang, F.M., Speziale, S., Shieh, S.R., Duffy, T.S., 2004. Single-crystal elasticity of andradite garnet to 11 GPa. *Journal of Physics-Condensed Matter* 16, S1041-S1052.

Kiseeva, E.S., Vasiukov, D.M., Wood, B.J., McCammon, C., Stachel, T., Bykov, M., Bykova, E., Chumakov, A., Cerantola, V., Harris, J.W., Dubrovinsky, L., 2018. Oxidized iron in garnets from the mantle transition zone. *Nature Geoscience* 11, 144-150.

Liu, Z., Gréaux, S., Cai, N., Siersch, N., Ballaran, T. B., Irifune, T., Frost, D. J., 2019. Influence of aluminum on the elasticity of majorite-pyrope garnets. *American Mineralogist* 104(7), 929-935.

Tappert, R., Stachel, T., Harris, J.W., Muehlenbachs, K., Ludwig, T., Brey, G.P., 2005. Diamonds from Jagersfontein (South Africa): messengers from the sublithospheric mantle. *Contributions to Mineralogy and Petrology* 150, 505-522.

Zhang, J.S., Bass, J.D., 2016. Single-crystal elasticity of natural Fe-bearing orthoenstatite across a high-pressure phase transition. Geophysical Research Letters 43, 8473-8481.